Coastal Engineering, 20 (1993) 29–58
Elsevier Science Publishers B.V., Amsterdam

Nonlinear evolution of a unidirectional shoaling wave field

Yehuda Agnon[a], Alexandru Sheremet[a], John Gonsalves[b] and Michael Stiassnie[a]
[a] *Faculty of Civil Engineering, Technion — Israel Institute of Technology, Haifa 32000, Israel*
[b] *Department of Mathematics, University of Port-Elizabeth, P.O. Box 1600, 6000 Port Elizabeth, South Africa*

(Received 4 May 1992; accepted after revision 19 November 1992)

ABSTRACT

Nonlinear energy transfer in the wave spectrum is very important in the shoaling region. Existing theories are limited to weakly dispersive situations (i.e. shallow water or narrow spectrum).

A nonlinear evolution equation for shoaling gravity waves is derived, describing the process all the way from deep to shallow water. The slope of the bottom is taken to be smaller, or of the order of the wave steepness (ϵ). The waves are assumed unidirectional for simplicity. The shoaling domain extends up to, and excluding, the first line of breaking of the waves. Reflection by the shore is neglected. Dispersion is fully accounted for.

The model equation includes terms due to quadratic interactions, which are effective over characteristic time and spatial scales of order (T/ϵ) and (λ/ϵ), respectively, where λ and T are wavelength and period at the spectral peak. In the limit of shallow water, the quadratic interaction model tends to the Boussinesq model.

By discretizing the wave spectrum, mixed initial and boundary value problems may be computed. The assumption of the existence of a steady state, transforms the problem into a boundary value one. For this case, solutions for a single triad of waves describing the subharmonic generation and for a full discretized spectrum were computed. The results are compared and found to be in good agreement with laboratory and field measurements. The model can be extended to directionally spread spectra and two dimensional bathymetry.

1. INTRODUCTION

As ocean waves shoal, the wave field undergoes substantial evolution from its deep water state. Narrow-band spectra develop secondary peaks at superharmonics of the peak frequency; broadband spectra show an increase of energy over a wide range of frequencies. A significant amount of energy is transferred to the long wave band. Phase velocities depart substantially from those predicted by the linear dispersion relation, and the shapes of individual waves change from almost symmetrical in deep water to ones with sharp crests and broad, flat troughs in shallow water.

Forecasting the wave spectrum in the shoaling region is of great importance

0378-3839/93/$06.00

to coastal and offshore engineering. The characteristic wave energy transfer to long period waves is associated with the observed phenomena of surf-beats and harbor oscillations which occur at low frequencies. Moored structures can also be resonated by the long waves. Edge waves, wave breaking and longshore currents and the resulting sediment transport are all sensitive to the form of the shoaled waves.

Linear theory, often used as a basis for shoaling models, does not predict most of these changes. Superposition of motions with different frequencies is used to satisfy arbitrary conditions at a given point. Locally, the wave number of each mode satisfies the linear dispersion relation. Separate components evolve separately, according to the conservation of energy equation at the lowest order. Although results proved to be roughly consistent (with errors up to 20%) with observations of r.m.s. shoaling waveheights, the most interesting features of the evolution described above, i.e. the effects of nonlinear energy transfer across the spectrum, are beyond the reach of the linear theory.

Considerable progress has been made in the last decade in the study of particular nonlinear evolution equations such as the Schrœdinger equation, Boussinesq and KdV-type equations.

Attempts to incorporate the effects of nonlinear interactions in shoaling models were also being made in two main directions: one based on Stokes expansions, involving cubic interactions, leading to Schrœdinger type equations; the second based on the assumption of shallow water, involving quadratic interactions and leading to Boussinesq-type equations.

Starting from previous work in similar nonlinear problems for the flat bottom case (Davey and Stewartson, 1974), Djordjevic and Redekopp (1978) used Stokes-type expansions of the velocity potential and free surface displacement to derive a cubic nonlinear evolution equation describing the evolution of the envelope of a gravity wave packet over uneven bottom.

Using more explicit conditions of a narrow spectrum and thus, weak dispersion, Stiassnie (1983) derived a similar equation starting from Whitham's set of modulation equations (Whitham, 1974). More recently, Suh et al. (1990) obtained an evolution equation for Stokes waves over mildly varying topography, including refraction, diffraction and nonlinear cubic interactions. In their work, the equations governing the water waves motion are perturbed using the method of multiple scales and Stokes expansions are used for the velocity potential and the free surface displacement.

In all these works the bottom slope is second order with respect to the wave steepness, the water is rather deep, dispersion is weak, and cubic interactions are the dominant energy exchange mechanism. Secondary waves are locked waves, as is the case in Laing (1986) where no energy exchange takes place.

Generalizations of Boussinesq and KdV equations to include the effects of sloping bottom were obtained by Peregrine (1967) and Grimshaw (1970). Using as a starting point the equation derived by Peregrine for the depth av-

eraged velocity potential and free surface displacement, Freilich and Guza (1984) derived two nonlinear models for the shoaling of unidirectional surface gravity waves, in the frequency domain. The models are valid in shallow water, and are weakly dispersive. The bottom slope is taken to be of the same order as the wave steepness.

All the above-mentioned works offer a description of the shoaling process restricted to a single mechanism of energy exchange - either cubic or quadratic interactions. In either case, dispersion is taken to be weak.

The shoaling process may be regarded as a transition process from cubic near resonance to quadratic near resonance. In deep water, cubic near resonance is dominant, with effects over characteristic time and spatial scales of order $O(T/\epsilon^2)$, $O(\lambda/\epsilon^2)$, λ and T being the wavelength and period of the spectral peak. Quadratic near resonance dominates the energy exchange in shallow water, effective over scales of order $O(T/\epsilon)$, $O(\lambda/\epsilon)$. As the water becomes shallow, quadratic resonance is approached, the second order forced waves grow and become free waves. The interaction is stronger and the spectrum widens. The spatial scale of interest here is λ/ϵ, hence cubic interaction is insignificant.

The aim of the present study is to derive an evolution equation describing the shoaling of wide spectra all the way from deep into shallow water, taking into account the full dispersion of the waves. For simplicity we are presenting a model for unidirectional waves at normal incidence on parallel depth contours. Extension to oblique incidence is straightforward. The cases of directionally spread spectra and more complex bathymetry can also be treated based on the present analysis.

In Section 2 we give the formulation of the problem. In Section 3 we derive the evolution equation. Section 4 presents the discretized equation and compares the model with Freilich and Guza's (1984) shallow water model. Examples of numerical integrations for a single triad of waves, and comparisons with laboratory experiments and field measurements are given in Sections 5 and 6, respectively.

2. FORMULATION OF THE PROBLEM

The equations governing the irrotational flow of an inviscid incompressible fluid with a free surface are:

$$\Delta\phi = 0 \qquad \text{for } h \le z \le \eta \tag{2.1}$$

$$\phi_z + \nabla_H h \cdot \nabla_H \phi = 0 \qquad \text{for } z = -h \tag{2.2}$$

$$\phi_{tt} + g\phi_z + (\nabla\phi)_t^2 + \tfrac{1}{2}\nabla\phi \cdot \nabla[(\nabla\phi)^2] = 0 \qquad \text{for } z = \eta \tag{2.3}$$

$$\phi_t + g\eta + \tfrac{1}{2}(\nabla\phi)^2 = 0 \qquad \text{for } z = \eta \tag{2.4}$$

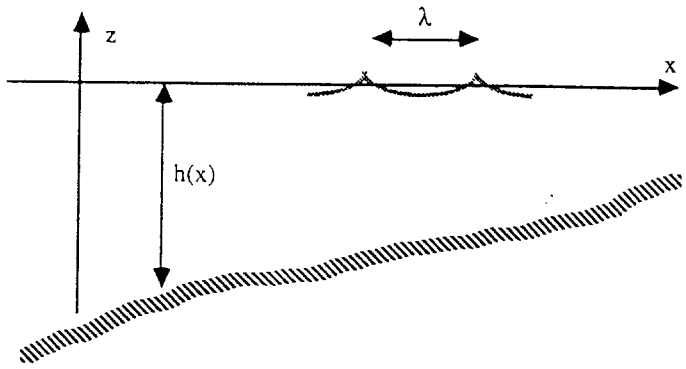

Fig. 1. The shoaling domain.

where ∇ and ∇_H are the three-dimensional and horizontal gradient operators and $\phi(x,y,z,t)$, $\eta(x,y,t)$ and $h(x,y)$ are the velocity potential, the free surface displacement and the water depth, respectively.

The reference frame has the origin at the still water level, in the deep water region, with the z axis pointing upwards, and the x axis pointing towards the shore (Fig. 1).

In order to derive an evolution equation for the shoaling of gravity waves, we impose the following restrictions:

(i) All depth contours are parallel to the shore-line. The waves propagate normally to the shore-line. Thus, the lateral coordinate y becomes irrelevant and may be dropped.

(ii) The shoaling domain under consideration extends from deep into shallow water, such that everywhere in the domain

$$kh = O(1) \tag{2.5}$$

where k is a typical wavenumber. The full dispersion of the waves has to be taken into account.

(iii) The small wave steepness parameter ϵ is introduced and it is assumed that wave breaking does not occur in this domain:

$$ka = O(\epsilon); \qquad \epsilon \ll 1 \tag{2.6}$$

where a is the amplitude of the wave.

(iv) The bottom slope is taken to be of the same order as the wave steepness:

$$h_x = O(\epsilon) \tag{2.7}$$

(v) Last, to simplify the problem, the reflected wave field is assumed to be of higher order than that taken into account here.

Next, the second "lateral" horizontal variable y is dropped, the governing equations (2.1–2.4) are scaled using relations (2.5–2.7) and terms of order $O(\epsilon^2)$ are neglected. For scaling purposes, the following nondimensional variables (primed) are introduced:

$$x' = k_0 x; \quad z' = k_0 z; \quad h' = k_0 h; \quad t' = \omega_0 t$$

$$\eta' = \frac{1}{a_0}\eta; \quad \phi' = \frac{\omega_0}{g a_0}\phi \tag{2.8}$$

$$\omega_0{}^2 = g k_0$$

k_0, a_0 and ω_0 are characteristic values for the wavenumber, amplitude and frequency of the wave field. The resulting dimensionless system of equations, after dropping the primes, is:

$$\phi_{xx} + \phi_{zz} = 0 \qquad \text{for } -h \leqslant z \leqslant \epsilon\eta \tag{2.9}$$

$$\phi_z + \epsilon h_x \phi_x = 0 \qquad \text{for } z = -h \tag{2.10}$$

$$\phi_{tt} + \phi_z + \epsilon[(\phi_x)^2 + (\phi_z)^2]_t = O(\epsilon^2) \qquad \text{for } z = \epsilon\eta \tag{2.11}$$

$$\phi_t + \eta + \tfrac{1}{2}\epsilon[(\phi_x)^2 + (\phi_z)^2] = 0 \qquad \text{for } z = \epsilon\eta \tag{2.12}$$

The surface η on which the last two boundary conditions are given is an unknown quantity. It is also a small perturbation of the still water level, and thus, a Taylor expansion about this level ($z=0$) is usually used to circumvent the above difficulty. The expansions for the boundary conditions at the free surface are:

$$\phi_{tt} + \phi_z + \epsilon\eta[\phi_{tt} + \phi_z]_z + \epsilon[(\phi_x)^2 + (\phi_z)^2]_t = O(\epsilon^2) \qquad \text{for } z = 0 \tag{2.13}$$

$$\phi_t + \eta + \epsilon\eta\phi_{tz} + \tfrac{1}{2}\epsilon[(\phi_x)^2 + (\phi_z)^2] = O(\epsilon^2) \qquad \text{for } z = 0 \tag{2.14}$$

The last relation may be used to eliminate η from the first, and after some simple algebra, system (2.9–2.12) becomes:

$$\phi_{xx} + \phi_{zz} = 0 \qquad \text{for } -h \leqslant z \leqslant 0 \tag{2.15}$$

$$\phi_z + \epsilon h_x \phi_x = 0 \qquad \text{for } z = -h \tag{2.16}$$

$$\phi_{tt} + \phi_z = \epsilon[-\tfrac{1}{2}(\phi_x)^2 - \tfrac{1}{2}(\phi_z)^2 + \phi_t\phi_{zt}]_t - \epsilon(\phi_x\phi_t)_x + O(\epsilon^2) \qquad \text{for } z = 0 \tag{2.17}$$

$$\eta = -\phi_t + \epsilon\phi_t\phi_{tz} - \tfrac{1}{2}\epsilon[(\phi_x)^{2+}(\phi_x)^2] + O(\epsilon^2) \qquad \text{for } z = 0 \tag{2.18}$$

The wave number spectrum representation is generally used to describe the evolution of a wave field. For the sloped bottom case it may also be used, together with a multiple scale approach, provided that the slope is small enough, but at the numerical integration stage problems arise in selecting the modes that enter the nonlinear interactions, due to the variation of the wave number with depth. To avoid this, the frequency domain representation will be used. Also, to account for the slow modulations induced by the depth variation and nonlinear interactions, slow variables are introduced:

$$x_1 = \epsilon x, \quad t_1 = \epsilon t \tag{2.19}$$

These slow variables are regarded formally as independent of the fast variables x and t. Accordingly, the derivatives become

$$\frac{\partial}{\partial x} \to \frac{\partial}{\partial x} + \frac{\partial}{\partial x_1} \quad \text{and} \quad \frac{\partial}{\partial t} \to \frac{\partial}{\partial t} + \frac{\partial}{\partial t_1} \tag{2.20}$$

The time Fourier transform of ϕ is defined as:

$$\Phi(\omega, t_1) = \int_{-\infty}^{\infty} \phi(t, t_1) e^{-i\omega t} dt$$

$$\phi(t, t_1) = \frac{1}{2\pi} \int_{-\infty}^{\infty} \Phi(\omega, t_1) e^{i\omega t} d\omega \tag{2.21}$$

With these, the Fourier transforms of Eqs. (2.15–2.17), to order $O(\epsilon)$ are:

$$\Phi_{xx} + \epsilon \Phi_{xx1} + \epsilon \Phi_{x1x} + \Phi_{zz} = O(\epsilon^2) \quad \text{for } h \le z \le 0 \tag{2.22}$$

$$\Phi_z + \epsilon h_{x_1} \Phi_x = O(\epsilon^2) \quad \text{for } z = -h \tag{2.23}$$

$$\begin{aligned} -\omega^2 \Phi + 2\epsilon i\omega \Phi_{t_1} + \Phi_z = -\frac{\epsilon i \omega}{4\pi} \int \int_{-\infty}^{\infty} \Big\{ & \Phi_x(\omega_1) \Phi_x(\omega_2) \\ & + \Phi_z(\omega_1) \Phi_z(\omega_2) + 2\omega_1 \omega_2 \Phi(\omega_1) \Phi_z(\omega_2) \\ & + 2\frac{\omega_2}{\omega} [\Phi_x(\omega_1) \Phi(\omega_2)]_x \Big\} \delta(\omega - \omega_1 - \omega_2) d\omega_1 d\omega_2 + O(\epsilon^2) \quad \text{for } z = 0 \end{aligned} \tag{2.24}$$

The system of Eqs. (2.22–2.24) is the starting point for the derivation of the evolution equation for shoaling gravity waves. It describes the evolution of the frequency spectrum Φ. The linear problem is represented by the left hand sides of the equations, while nonlinear interaction among the modes is accounted for by the nonlinear convolution integral on the right hand side of Eq. (2.24).

In the sequel, in order to make the formulae more easy to follow, the variables on which the functions depend will generally not appear. They will be indicated if significant, and only where confusion may arise.

3. DERIVATION OF THE EVOLUTION EQUATION

In order to obtain a single evolution equation, we shall first look for a so-

lution of the Laplace equation (2.22) together with the bottom boundary condition (2.23). The solution for this problem may be formally written as a superposition of two different kinds of terms: one representing the free waves, the other associated with locked waves.

The free wave part of $\Phi(\omega)$ has the form:

$$F(x_1,z,\omega,t_1)\mathrm{e}^{-i\theta}$$

where

$$\theta=\int_0^x k(x_1,\omega)\mathrm{d}x; \quad k \text{ real} \tag{3.1}$$

where k is the free wave number and satisfies the linear dispersion relation:

$$\omega^2=k\tanh(kh) \tag{3.2}$$

The free wave (Eqs. 3.1–3.2) is the solution of the linear approximation of the system (2.22–2.24).

The locked wave terms generated by two forcing free waves have the form:

$$F'(x_1,z,\omega,t_1,\omega_1,\omega_2)\mathrm{e}^{-i\theta'}$$

$$\theta'=\int_0^x k'(x_1,\omega_1,\omega_2)\mathrm{d}x; \quad k' \text{ real} \tag{3.3}$$

where k' does not satisfy the linear dispersion relation (3.2). The frequencies ω_1, ω_2 correspond to the forcing free waves. Locked waves forced by more than two free waves will not be taken into account, since they correspond to higher order nonlinear terms (cubic interactions) neglected in this study.

A measure of the departure of Eq. (3.3) from the free wave character is given by the detuning parameter:

$$\mu=(k'-k)/k \tag{3.4}$$

where k is given by Eq. (3.2) with $\omega=\omega_1+\omega_2$. In deep water μ is of order unity and the locked wave is of second order. As the depth decreases, μ approaches zero, resonance conditions are approached and the locked wave becomes in effect a first order free wave. Thus, the order of the locked wave will be taken in the sequel to be:

$$F'=\mathrm{O}(\epsilon/\mu) \tag{3.5}$$

all along the shoaling region.

Using the fact that the locked waves arise in deep water as forced waves given by the convolution integrals in Eq. (2.24), we shall look for the solution

of the Laplace equation with the bottom boundary condition (Eqs. 2.22 and 2.23) in the form:

$$\Phi = F(x_1,z,\omega,t_1)\mathrm{e}^{-i\theta} + \Phi'$$

$$\theta = \int_0^x k(x_1,\omega)\mathrm{d}x \tag{3.6}$$

$$\omega^2 = k\tanh(kh)$$

where Φ' denotes the locked wave associated with the frequency ω and is given by:

$$\Phi' = \int_{-\infty}^{\infty}\int F'(x_1,z,\omega,t_1,\omega_1,\omega_2)e^{-i\theta'}\delta(\omega-\omega_1-\omega_2)\mathrm{d}\omega_1\,\mathrm{d}\omega_2$$

$$\theta' = \int_0^x k'(x_1,\omega_1,\omega_2)dx; \quad k'(x_1,\omega_1,\omega_2) = k(x_1,\omega_1,\omega_2) \tag{3.7}$$

In view of the linearity of the present problem, upon substitution of Eqs. (3.6) and (3.7) into Eqs. (2.22) and (2.23), two systems of equations having similar form may be separated, one for the free wave:

$$\begin{aligned} &F_{zz} - k^2F - \epsilon i(kF)_{x_1} - \epsilon ikF_{x_1} = \mathrm{O}(\epsilon^2) && \text{for } -h \le z \le 0 \\ &F_z - \epsilon ikh_{x_1}F = \mathrm{O}(\epsilon^2) && \text{for } z-h \end{aligned} \tag{3.8}$$

and one for the locked wave, obtained by replacing k and F by k′ and F′, respectively, in Eq. (3.8). The details of solving this system are given in the Appendix. The solution for the velocity potential is:

$$\Phi = \left[\frac{\varphi(x_1,\omega,t_1)}{\cosh(kh)}\cosh k(z+h) + \epsilon D(k,z)\cdot\frac{\varphi(x_1,\omega,t_1)}{\cosh(kh)}\right]\mathrm{e}^{-i\theta}$$

$$+\int_{-\infty}^{\infty}\int\left[\frac{\varphi'(x_1,\omega,t_1,\omega_1,\omega_2)}{\cosh(k'h)}\cosh(k'(z+h)) + \epsilon D(k',z)\left(\frac{\varphi'(x_1,\omega,t_1,\omega_1,\omega_2)}{\cosh(k'h)}\right)\right]$$

$$\cdot\mathrm{e}^{-i\theta'}\cdot\delta(\omega-\omega_1-\omega_2)\mathrm{d}\omega_1\,\mathrm{d}\omega_2 \tag{3.9}$$

where φ and φ' are unknown functions, and the operator $D(k,z)$ is defined by:

$$D(k,z) = i\left[(z+h)\sinh(k(z+h))\frac{\partial}{\partial x_1} + \frac{1}{2}(k(z+h)^2)_{x_1}\cosh k(z+h)\right] \tag{3.10}$$

and

$$D_z \equiv \frac{\partial D}{\partial z}$$

At this stage, it should be noted that, to first order, the potential on $(z=0)$ is:

$$\Phi|_{z=0} = \varphi(x_1,\omega,t_1)e^{-i\theta} + \int\int_{-\infty}^{\infty} \varphi'(x_1,\omega,t_1,\omega_1,\omega_2)e^{-i\theta'}\ \delta(\omega-\omega_1-\omega_2)\,d\omega_1\,d\omega_2 \tag{3.11}$$

and is equal, to an error of $O(\epsilon)$, to the free surface velocity potential, denoted here by Ψ:

$$\Psi = \Phi|_{z=\epsilon\eta} = \Phi|_{z=0} + O(\epsilon) \tag{3.12}$$

Next, we substitute the solution (3.9–3.10) into the surface boundary condition (2.24). The contribution of the free waves to the left hand side of Eq. (2.24) is:

$$-\omega^2\left[\varphi + \epsilon D(k,0)\left(\frac{\varphi}{\cosh(kh)}\right)\right]e^{-i\theta} + 2\epsilon i\omega\phi_{t_1}e^{-i\theta}$$
$$+\left[\varphi k\tanh(kh) + \epsilon D_z(k,0)\left(\frac{\varphi}{\cosh(kh)}\right)\right]e^{-i\theta} \tag{3.13}$$

The contribution of the "locked" waves to the left hand side of Eq. (2.24) is:

$$-\omega^2\int\int_{-\infty}^{\infty}\left[\varphi' + \epsilon D(k',0)\left(\frac{\varphi'}{\cosh(k'h)}\right)\right]e^{-i\theta'}\delta(\omega-\omega_1-\omega_2)\,d\omega_1\,d\omega_2$$

$$+2\epsilon i\omega\int\int_{-\infty}^{\infty}\varphi'_{t_1}e^{-i\theta'}\delta(\omega-\omega_1-\omega_2)\,d\omega_1\,d\omega_2$$

$$+\int\int_{-\infty}^{\infty}\left[\varphi' k'\tanh(k'h) + \epsilon D_z(k',0)\left(\frac{\varphi'}{\cosh(k'h)}\right)\right]e^{-i\theta'}$$
$$\cdot\delta(\omega-\omega_1-\omega_2)\,d\omega_1\,d\omega_2 \tag{3.14}$$

We now make use of the linear dispersion relation (3.2), denote also:

$$\Omega^2 = k'\tanh(k'h) \tag{3.15}$$

and expand in Taylor series about k:

$$D(k',0)\left(\frac{\varphi'}{\cosh(k'h)}\right)=D(k,0)\left(\frac{\varphi'}{\cosh(kh)}\right)+O(\mu)$$

$$D_z(k',0)\left(\frac{\varphi'}{\cosh(k'h)}\right)=D_z(k,0)\left(\frac{\varphi'}{\cosh(kh)}\right)+O(\mu) \tag{3.16}$$

With these, gathering together the relations (3.13) and (3.14), we obtain for the left hand side of Eq. (2.24) the expression:

$$2\epsilon i\omega[\varphi e^{-i\theta}+\int_{-\infty}^{\infty}\int\varphi' e^{-i\theta'}\delta(\omega-\omega_1-\omega_2)d\omega_1 d\omega_2]_{t_1}-\epsilon\omega^2 D(k,0)$$

$$\cdot\left\{\frac{1}{\cosh(kh)}[\varphi e^{-i\theta}+\int_{-\infty}^{\infty}\int\varphi' e^{-i\theta'}\delta(\omega-\omega_1-\omega_2)d\omega_1 d\omega_2]\right\}$$

$$+\epsilon D_z(k,0)\cdot\left\{\frac{1}{\cosh(kh)}[\varphi e^{-i\theta}+\int_{-\infty}^{\infty}\int\varphi' e^{-i\theta'}\delta(\omega-\omega_1-\omega_2)\quad d\omega_1 d\omega_2]\right\}$$

$$+\int_{-\infty}^{\infty}\int(\Omega^2-\omega^2)\varphi' e^{-i\theta'}\delta(\omega-\omega_1-\omega_2)d\omega_1 d\omega_2 \tag{3.17}$$

We may use now Eq. (3.12), setting

$$\Psi=\varphi e^{-i\theta}+\int_{-\infty}^{\infty}\int\varphi' e^{-i\theta'}\delta(\omega-\omega_1-\omega_2)d\omega_1 d\omega_2+O(\epsilon) \tag{3.18}$$

and upon substitution into Eq. (3.17) obtain for the left hand side of Eq. (2.24):

$$2\epsilon i\omega\Psi_{t_1}+\epsilon[-\omega^2 D(k,0)+D_z(k,0)]\left(\frac{\Psi}{\cosh(kh)}\right)$$

$$+\int_{-\infty}^{\infty}\int(\Omega^2-\omega^2)\varphi' e^{-i\theta'}\delta(\omega-\omega_1-\omega_2)d\omega_1 d\omega_2 \tag{3.19}$$

But, by way of simple algebra, it may be shown that:

$$[-\omega^2 D(k,0)+D_z(k,0)]\cdot\frac{1}{\cosh(kh)}=i\omega\left[C_{g,x_1}+2C_g\frac{\partial}{\partial x_1}\right] \tag{3.20}$$

where $C_g=(\partial k/\partial \omega)^{-1}$ is the group velocity of the free wave, so that the expression (3.19) becomes:

$$2\epsilon i\omega[\Psi_{t_1}+\tfrac{1}{2}C_{g,x_1}\Psi+C_g\Psi_{x_1}]$$

$$+\int_{-\infty}^{\infty}\int(\Omega^2-\omega^2)\varphi' e^{-i\theta'}\delta(\omega-\omega_1-\omega_2)d\omega_1 d\omega_2 \tag{3.21}$$

Finally, further simplification may be made. A Taylor expansion of Ω^2 about k gives:

$$\Omega^2-\omega^2=2\omega C_g(k'-k)+O(\mu^2) \tag{3.22}$$

We shall replace Ω^2 by this expression and gather the last term and the term containing the derivative of Ψ in Eq. (3.21):

$$2i\omega C_g\left\{\epsilon\varphi_{x_1}e^{-i\theta}+\int_{-\infty}^{\infty}\int[\epsilon\varphi_{x_1}-i(k'-k)\varphi']e^{-i\theta'}\delta(\omega-\omega_1-\omega_2)d\omega_1 d\omega_2\right\}$$

$$=2i\omega C_g e^{-i\theta}\left\{\epsilon\varphi_{x_1}+\int_{-\infty}^{\infty}\int[\epsilon\varphi'_{x_1}-i(k'-k)\varphi']e^{-i(\theta'-\theta)}\delta(\omega-\omega_1-\omega_2)d\omega_1 d\omega_2\right\}$$

$$+O(\epsilon\mu) \tag{3.23}$$

We may return now to a single scale spatial variable x, and write:

$$\Psi(x,\omega,t_1)=A(x,\omega,t_1)e^{-i\theta} \tag{3.24}$$

It may be seen that the expression in the last curled brackets in Eq. (3.23) is the spatial derivative of A. The left hand side of Eq. (2.24) then takes the simple form:

$$2\epsilon i\omega(A_{t_1}+\tfrac{1}{2}C_{g,x}A+C_gA_x)e^{-i\theta} \tag{3.25}$$

In dealing with the second order nonlinear right hand side of Eq. (2.24), only the leading order free and locked wave components need to be taken into account:

$$\Phi=\varphi\frac{\cosh k(z+h)}{\cosh kh}e^{-i\theta}+\int_{-\infty}^{\infty}\int\varphi'\frac{\cosh k'(z+h)}{\cosh k'h}e^{-i\theta} \tag{3.26}$$

$$\delta(\omega-\omega_1-\omega_2)d\omega_1 d\omega_2+O(\epsilon)$$

For the derivatives of Φ we may write, using Eqs. (3.11), (3.12) and (3.5):

$$\Phi_z|_{z=0}=\omega^2\Psi+O(\epsilon) \tag{3.27}$$

$$\Phi_z|_{z=0}=-ik\Psi+O(\epsilon) \tag{3.28}$$

and returning to Eq. (2.24) we obtain for its right hand side:

$$2\epsilon i\omega \int_{-\infty}^{\infty}\int V(\omega,\omega_1,\omega_2)\Psi(\omega_1)\Psi(\omega_2)\delta(\omega-\omega_1-\omega_2)\mathrm{d}\omega_1\,\mathrm{d}\omega_2 \tag{3.29}$$

where the kernel V brought to a symmetric form, is given by:

$$V(\omega,\omega_1,\omega_2)=\frac{1}{4\pi}\left[2k_1k_2+(\omega_1\omega_2)^2+k_1^2\frac{\omega_2}{\omega}+k_2^2\frac{\omega_1}{\omega}-\omega^2\omega_1\omega_2\right] \tag{3.30}$$

It is readily seen that the kernel has the properties:

$$V(\omega,\omega_1,\omega_2)=V(\omega,\omega_2,\omega_1)$$
$$V(-\omega,-\omega_1,-\omega_2)=V(\omega,\omega_1,\omega_2) \tag{3.31}$$

Finally, collecting together Eqs. (3.25), (3.29) and (3.30) we obtain the equation:

$$A_{t_1}(\omega)+\tfrac{1}{2}C_{g,x}A(\omega)+C_gA_x(\omega)$$
$$=\int_{-\infty}^{\infty}\int V(\omega,\omega_1,\omega_2)A(\omega_1)A(\omega_2)\mathrm{e}^{-i(\theta-\theta_1-\theta_2)}\delta(\omega-\omega_1-\omega_2)\mathrm{d}\omega_1\,\mathrm{d}\omega_2$$
$$+\mathrm{O}(\epsilon^2,\mu\epsilon) \tag{3.32}$$

Equation (3.32), the main result of this study, is an evolution equation, in the frequency domain, for shoaling gravity wave fields of arbitrary spectra, valid for a domain that extends all the way from deep to shallow water. As seen from the approximations used in Eqs. (3.16) and (3.22), over time and length scales of order $\mathrm{O}(\epsilon^{-1})$, it describes the free waves with a relative error of order $\mathrm{O}(\epsilon)$ and the locked waves with a relative error of $\mathrm{O}(\mu)$.

From Eq. (3.32) we may derive the next order approximation to the linear theory energy conservation equation. By multiplying Eq. (3.32) by the complex conjugate of A and adding to the result its complex conjugate and replacing A by the modal wave amplitude a:

$$a=-i\omega A \tag{3.33}$$

we obtain the equation:

$$(|a|^2)_{t_1}+(C_g\cdot|a|^2)_x=-\int_{-\infty}^{\infty}\int 2\frac{\omega_1\omega_2}{\omega}V(\omega,\omega_1,\omega_2)\mathrm{Im}[a^*(\omega)a(\omega_1)a(\omega_2)\mathrm{e}^{-i(\theta-\theta_1-\theta_2)}]$$
$$\cdot\delta(\omega-\omega_1-\omega_2)\mathrm{d}\omega_1\,\mathrm{d}\omega_2 \tag{3.34}$$

where Im[ ] is the imaginary part, and the asterisk denotes the complex conjugate.

The left-hand side of Eq. (3.34) represents translation of the wave energy, which has density $|a|^2/2$. The right-hand side is due to nonlinear (quadratic) interaction. Its role is to redistribute the energy across the spectrum. In order to carry out computations, we shall now discretize the evolution equation (3.32).

4. DISCRETIZATION AND COMPARISON WITH THE BOUSSINESQ MODEL

In this section we discretize the evolution equation (3.32) and show that in the limit of shallow water it reduces to the modal form of the Boussinesq model of Freilich and Guza (1984). The model we obtain is in a form suitable for numerical computations of the evolution of wave spectra in discretized form. We shall express the surface velocity potential as a Fourier series:

$$\Psi(x,t,t_1)=\varphi(x,z=\eta,t,t_1)=-\frac{i}{2}\sum_{j=-\infty}^{\infty}A_j(x,t_1)\mathrm{e}^{i(\theta_j-\omega_j t)} \tag{4.1}$$

where:

$$A_{-j}=A_j^*;\quad \omega_{-j}=-\omega_j$$

$$\theta_j=\int_0^x k_j\mathrm{d}x;\quad k_j=k(x_1,\omega_j)$$

$$\omega_j^2=k_j\tanh(k_jh) \tag{4.2}$$

and restrict the problem to unidirectional waves propagating towards the shore by imposing:

$$k_j\omega_j>0 \tag{4.3}$$

The Fourier transform of Eq. (4.1) gives an expansion for the amplitude A in the form:

$$A(x,\omega,t_1)=-i\pi\sum_{j=-\infty}^{\infty}A_j(x,t_1)\delta(\omega+\omega_j) \tag{4.4}$$

If this expression is substituted into Eq. (3.32), integrations over ω_1, ω_2 are performed and use is made of the symmetry properties of the kernel (Eq. 3.31), the following equation is obtained:

$$\sum_{j=-\infty}^{\infty}(A_{j,t_1}+\tfrac{1}{2}C_{\mathrm{g}jx}A_j+C_{\mathrm{g}j}A_{jx})\delta(\omega+\omega_j)=$$

$$-i\sum_{\alpha,\beta=-\infty}^{\infty}\pi V(\omega,\omega_\alpha,\omega_\beta)A_\alpha A_\beta\mathrm{e}^{-i(\theta-\theta_\alpha-\theta_\beta)}\delta(\omega+\omega_\alpha+\omega_\beta) \tag{4.5}$$

Then, by identifying the terms with identical δ functions, one obtains the system:

$$A_{j,t_1}+\tfrac{1}{2}C_{g,jx}A_j+C_{g,j}A_{jx}=-i\sum_{\alpha,\beta=-\infty}^{\infty}\pi V(\omega_j,\omega_\alpha,\omega_\beta)A_\alpha A_\beta e^{-i(\theta_j-\theta_\alpha-\theta_\beta)}$$

$$\delta(\omega_j-\omega_\alpha-\omega_\beta)\quad \text{for all integer } j \tag{4.6}$$

which may be restricted to only positive indices, using relations (4.2) and (4.3) and the symmetry of the kernel. The result is the discretized variant of Eq. (3.32):

$$A_{j,t_1}+\tfrac{1}{2}C_{g,jx}A_j+C_{g,j}A_{jx}=$$

$$-i\sum_{\alpha,\beta=1}^{\infty}\pi V(\omega_j,\omega_\alpha,\omega_\beta)A_\alpha A_\beta e^{-i(\theta_j-\theta_\alpha-\theta_\beta)}\delta(\omega_j-\omega_\alpha-\omega_\beta)$$

$$+i\sum_{\alpha,\beta=1}^{\infty}2\pi V(\omega_j,-\omega_\alpha,\omega_\beta)A_\alpha^* A_\beta e^{-i(\theta_j+\theta_\alpha-\theta_\beta)}\delta(\omega_j+\omega_\alpha-\omega_\beta)\quad j=1,2,... \tag{4.7}$$

The inclusion of A_0, a drift current and set down potential requires special attention and is not presented here. Applying the model to waves on a beach, we may use a zero mean mass flux argument to show that the drift current is $O(\epsilon)$.

Equation (4.7) enables a comparison with the model derived by Freilich and Guza (1984) for shoaling of gravity waves in shallow water. In the shallow water domain:

$$(kh)^2=O(\epsilon) \tag{4.8}$$

so that the following expansions may be used:

$$\begin{aligned} k_j&=k_{0j}+k_{1j}+O(\epsilon^2)\\ k_{0j}&=\omega_j h^{-1/2}\\ k_{1j}&=\tfrac{1}{6}\omega_j{}^3 h^{-1/2}\end{aligned} \tag{4.9}$$

and

$$\begin{aligned} C_{gj}&=h^{1/2}+O(\epsilon)\\ (\omega_\alpha\omega_\beta)^2&=O(\epsilon)\end{aligned} \tag{4.10}$$

With these, to leading order, the kernels of (4.7) become

$$\pi V(\omega_j,\omega_\alpha,\omega_\beta)=\frac{3}{8h}\omega_\alpha\omega_\beta \tag{4.11}$$

Following Freilich and Guza (1984), the corrected wave number is:

$$T_j = k_{1j} + \kappa_j \tag{4.12}$$

where κ_j, the first order nonlinear correction to the wave number, is defined by:

$$A_j = |A_j| \exp\left(i \int_0^x \kappa_j \mathrm{d}x \right) = |A_j| \exp\left(i \int_0^x (T_j - k_{1j}) \mathrm{d}x \right) \tag{4.13}$$

and introduce the truncated total phase:

$$\Theta = \int_0^x (k_{0j} + T_j) \mathrm{d}x + \mathrm{O}(\epsilon^2) \tag{4.14}$$

For a steady state ($A_{t_1} = 0$), the following system is obtained:

$$\begin{aligned}
&\left(|A_j|_x + \tfrac{1}{4} \frac{h_x}{h} |A_j| \right) + i |A_j| (T_j - k_{1j}) = \\
&\quad - i \sum_{\alpha,\beta=1}^{\infty} \frac{3h^{-3/2}}{8} \omega_\alpha \omega_\beta |A_\alpha| |A_\beta| \mathrm{e}^{-i(\Theta_j - \Theta_\alpha - \Theta_\beta)} \delta(\omega_j - \omega_\alpha - \omega_\beta) \\
&\quad - i \sum_{\alpha,\beta=1}^{\infty} \frac{3h^{-3/2}}{8} \omega_\alpha \omega_\beta |A_\alpha| |A_\beta| \mathrm{e}^{-i(\Theta_j + \Theta_\alpha - \Theta_\beta)} \delta(\omega_j + \omega_\alpha - \omega_\beta) \\
&\quad - i \sum_{\alpha,\beta=1}^{\infty} \frac{3h^{-3/2}}{8} \omega_\alpha \omega_\beta |A_{\bar{\alpha}}| |A_\beta| \mathrm{e}^{-i(\Theta_j - \Theta_\alpha + \Theta_\beta)} \delta(\omega_j - \omega_\alpha + \omega_\beta)
\end{aligned} \tag{4.15}$$

Separation of the real and imaginary parts of Eq. (4.15) yields Freilich's consistent shoaling model.

In order to solve Eq. (3.32) or its discrete counterpart Eq. (4.7), suitable initial and boundary conditions have to be set. They amount to specifying the energy flux spectrum at the boundary of the shoaling region at any time, together with the initial wave field inside the domain. In the present study, the simpler case of steady state was considered. Assuming that the amplitudes do not depend on the slow time t_1, system Eq. (4.7) becomes:

$$\begin{aligned}
&\tfrac{1}{2} C_{g,jx} A_j + C_{g,j} A_{jx} = - i \sum_{\alpha,\beta=1}^{\infty} \pi V(\omega_j, \omega_\alpha, \omega_\beta) A_\alpha A_\beta \mathrm{e}^{-i(\theta_j - \theta_\alpha - \theta_\beta)} \delta(\omega_j - \omega_\alpha - \omega_\beta) \\
&\quad + i \sum_{\alpha,\beta=1}^{\infty} 2\pi V(\omega_j, -\omega_\alpha, \omega_\beta) A_\alpha^* A_\beta \mathrm{e}^{-i(\theta_j - \theta_\alpha - \theta_\beta)} \delta(\omega_j + \omega_\alpha - \omega_\beta)
\end{aligned} \tag{4.16}$$

where

$$A_j = A(x,\omega_j)$$

$$C_{g,j} = \left(\frac{\partial k}{\partial \omega}\right)^{-1}_{\omega=\omega_j}$$

$$\theta_j = \int_0^x k(x,\omega_j)\,\mathrm{d}x, \quad j=1,2,...$$

which is an ordinary nonlinear differential system of equations. Specification of the modal amplitude and phases at the deep water end of the domain will serve as a boundary condition and integration may be carried out to obtain the shoaled spectrum at an arbitrary depth.

Equation (4.16) has no known analytical solutions. If the water is of constant depth and only a single triad with suitably chosen frequencies is considered, Armstrong et al. (1962) and Bretherton (1964) have shown that analytical solutions may be found for the modal amplitude and phase variations in terms of Jacobi elliptic functions.

In the present study, Eq. (4.16) was integrated using solvers from the mathematical library IMSL. The numerical algorithm, known as "repeated rational extrapolation to the limit" is due to Burlisch and Stoer (1966). The algorithm keeps the global error proportional to the user-specified tolerance, and was used to check the accuracy of our results. It is claimed by its authors and by Freilich and Guza (1984) to be less time consuming than the methods of Runge–Kutta, Adams–Moulton–Bashforth or the corresponding extrapolation method that uses polynomials. We have used the Adams–Moulton–Bashford method, which we found to be somewhat less time consuming for the bulk of our computations.

The accuracy of the scheme was tested for the case of a single triad composed of twice the same wave and its second harmonic, over even bottom, for different depths. The results agreed with the analytical solution, available in this case. The first order energy flux was also monitored for all numerical integrations. It never varied by more than 3% along the whole integration domain.

5. NUMERICAL SOLUTIONS FOR A TRIAD OF WAVES

In order to assess the performance of the present model, we consider as a first test the nonlinear evolution of a system consisting of only three waves with frequencies chosen to describe difference interactions:

$$\omega_1 = \frac{1}{120}\,\text{Hz}$$

$$\omega_2 = n\omega_1$$

$$\omega_3 = (n+1)\omega_1; \quad n \text{ integer} \tag{5.1}$$

such that ω_1, ω_2, ω_3 satisfy the relation:

$$\omega_1 + \omega_2 - \omega_3 = 0 \tag{5.2}$$

For the case of a single triad given by Eqs. (5.1) and (5.2) the system of Eq. (4.16) becomes:

$$\tfrac{1}{2}C_{g1x}A_1 + C_{g1}A_{1x} = 2i\pi V(\omega_1, -\omega_2, \omega_3)A_2^* A_3 e^{-i\Delta\theta}$$

$$\tfrac{1}{2}C_{g2x}A_2 + C_{g2}A_{2x} = 2i\pi V(\omega_2, -\omega_1, \omega_3)A_1^* A_3 e^{-i\Delta\theta}$$

$$\tfrac{1}{2}C_{g3x}A_3 + C_{g3}A_{3x} = -2i\pi V(\omega_3, \omega_1, \omega_2)A_1 A_2 e^{-i\Delta\theta}$$

with

$$\Delta\theta = \theta_3 - \theta_1 - \theta_2$$

$$\theta_i = \int_0^x k(x,\omega_i)\,dx; \quad i = 1,2,3 \tag{5.3}$$

The parameters expected to affect the solution are the slope of the bottom, the initial amplitudes of the waves and the initial relative phase. In all the integrations performed the initial value for the complex amplitude of the long wave (wave "1") was taken as the corresponding locked wave, forced by the shorter waves "2" and "3", as given by Eqs. (5.3). If the water is deep enough, the assumption that the long wave is of higher order holds; the shorter waves evolve on slower spatial scales (the right hand sides of the corresponding equations in Eqs. (5.3) are of higher order). Then, the first equation in Eqs. (5.3) may be integrated, yielding:

$$C_{g1}^{1/2}A_1 = -2\pi\frac{V(\omega_1, -\omega_2, \omega_3)}{k_3 - k_1 - k_2}A_2^* A_3 e^{-i\Delta\theta} \tag{5.4}$$

The use of Eq. (5.4) for the initialization of the long wave may be shown to make the initial relative phase of the system irrelevant and thus, the relevant parameters remain the slope and the initial amplitudes. It should also be noted here that Eqs. (5.3) for a single triad should keep the first order energy flux constant within an error of $O(\epsilon)$. In deep water, the primary waves evolution is governed by the linear energy conservation law while the secondary wave is locked and its contribution is to the next order. In shallow water on the other hand, using the Boussinesq-type asymptotic form of Eqs. (5.3) it

may be shown that the energy is exactly conserved. From the same analysis one obtains that the wave action is not conserved, in agreement with results cited by Phillips (1977).

The integrations performed comprise two groups: one dealing with the comparison of the present model with other models; the other with the influence of the mentioned parameters on the numerical results.

For comparison with other models, the bottom slope was fixed at 0.01. In all cases, the initial amplitudes of waves 2 and 3 were the same:

$$a_j = \frac{\omega}{g} A_j = 1 \text{ m}; \quad j = 2,3 \tag{5.5}$$

For the linear model, the evolution of the waves "2" and "3" is computed using the linear energy conservation law:

$$(A_j \cdot C_{gj}^{1/2})_x = 0; \quad j = 2,3 \tag{5.6}$$

and the long wave "1" is computed locally by means of relation (5.4). Comparison with the linear model was made over a depth span from 50 m to 3 m.

Figure 2 compares the results of the present model (solid lines) with the linear one (dashed lines). The shorter waves have an amplitude of 1 m in deep water (2 and 3). In deep water, the present model keeps the long wave constant to order $O(\epsilon)$ and almost no energy is exchanged with the primary waves: the long wave is in effect a forced locked wave. As the water becomes shallow, the linear model exhibits a very fast growth of the long wave. An asymptotic expansion based on the assumption that it remain of order $O(\epsilon)$ breaks down here. In the present model, this is the region where the secondary wave begins to affect the primary waves, and energy exchange among the triad becomes important. The long wave remains finite.

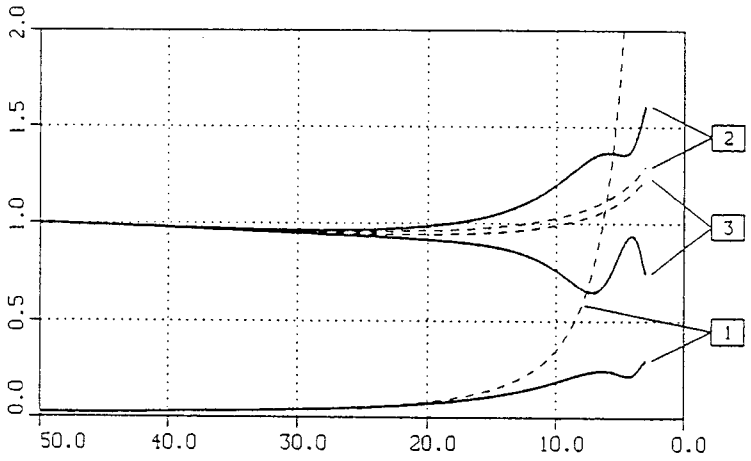

Fig. 2. Shoaling of a triad of waves. Comparison of the present model (full line) with the linear model (dashed line), for medium waves.

The result of Freilich and Guza's (1984) Boussinesq-type consistent shoaling model is given in Eq. (4.15), and is expected to perform well in shallow water. For comparison purposes, the present model was started at 20 m depth, and its results at water depth of 15 m were taken as initial conditions for the Boussinesq-type shoaling model. Values characteristic for short, medium and long waves were taken as follows:

$$\begin{aligned} &\text{Short waves:} && n=20; && \omega_2=\tfrac{1}{6}\text{Hz}; && \lambda_2\approx 55\text{ m} \\ &\text{Medium waves:} && n=12; && \omega_2=\tfrac{1}{10}\text{Hz}; && \lambda_2\approx 130\text{ m} \\ &\text{Long waves:} && n=7; && \omega_2=\tfrac{1}{17.1}\text{Hz}; && \lambda_2\approx 250\text{ m} \end{aligned} \tag{5.7}$$

where the wavelength of wave 2 is given at the depth $h=20$ m as calculated by the linear dispersion relation.

Figure 3 shows the performance of the present model (solid lines) against the Boussinesq model given in Eq. (4.15) (dashed lines). As it should be expected, the agreement is best for the long wave case and worst for the short wave one.

The influence of the bottom slope and the initial amplitudes on the solutions of Eqs. (5.3) is shown in Fig. 4. The integrations were performed for medium length waves, as defined in Eq. (5.7).

For the study of the influence of the bottom slope, the initial amplitudes of the primary waves were 1 m. For these integrations, the domain was reduced to water of depth less than 20 m as up to that depth it has been seen previously that the linear model gives relatively accurate results (the secondary long-wave has a forced wave status).

Most common values for beach slopes lie between 0.005 and 0.05. The solution for these two values are shown in Fig. 4a. The evolution on a slope of 0.05 (dashed line) is compared with the evolution on a very mild slope of 0.005 (solid curve) on a milder slope the horizontal distance (and time) for interaction is longer. This results in more intensive interaction over the specified depth range. Hence the oscillations in the waves' amplitudes. For the study of the influence of the initial amplitude, the slope was fixed at a value of 0.01. In Fig. 4b we compare the interaction of medium waves with 1 m deep-water amplitude (dashed lines) to waves with 2 m amplitude (solid curves). The higher waves interact more strongly, giving rise to more rapid oscillations in their amplitudes. Note that the accompanying long wave becomes relatively higher in shallow water. It becomes proportional to ϵ rather than ϵ^2 as it changes from a forced wave to a free wave. The secondary long wave is initially 4 times greater in the second case than in the first case. At the end of the shoaling region, at depth of 3 m, their ratio is about 2. Thus, we see that the importance of nonlinear interaction increases on milder slopes and with steeper waves.

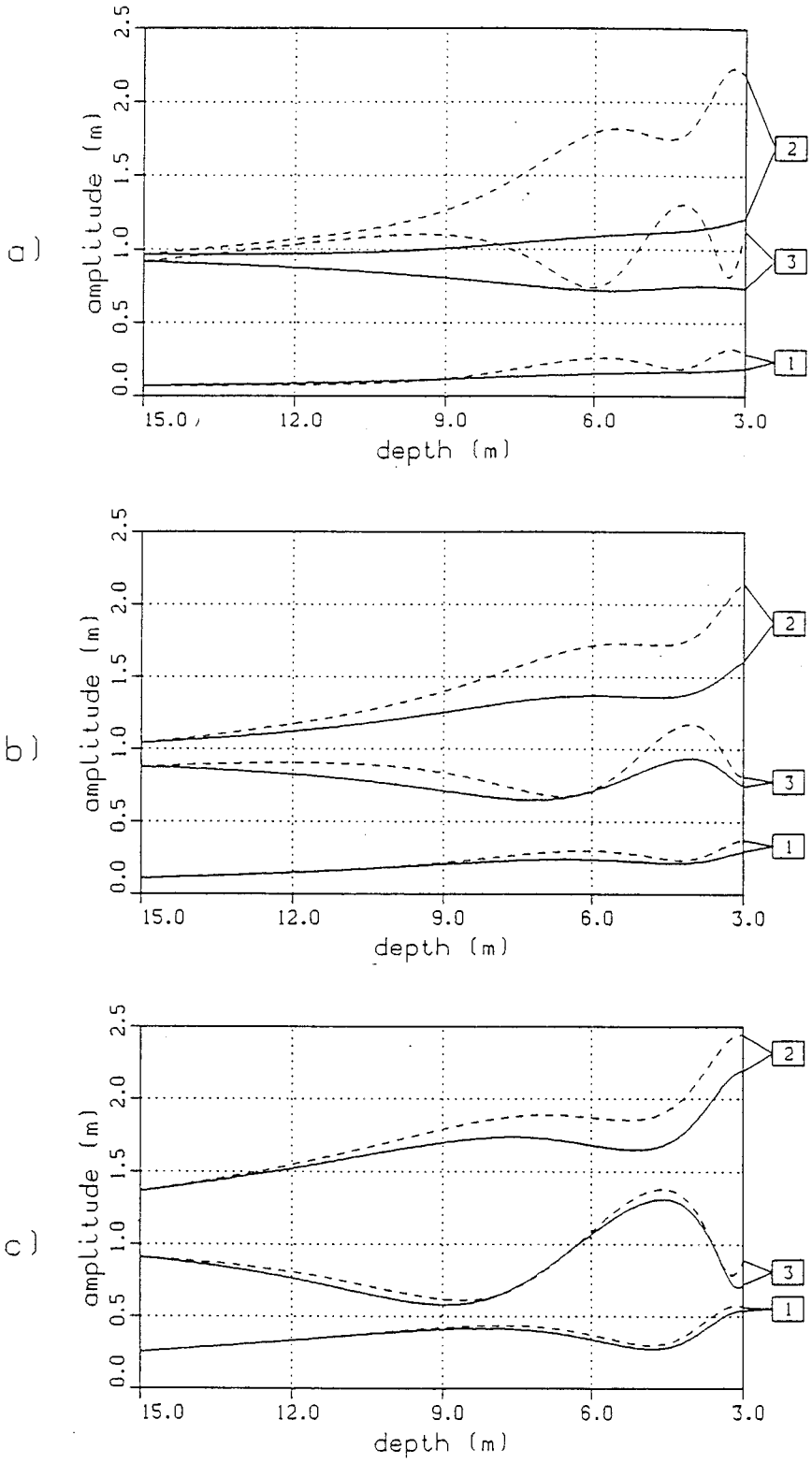

Fig. 3. Shoaling of a triad of waves. Comparison of the present model (full line) with the Boussinesq-type model of Freilich and Guza (1984) (dashed line). (a) short waves; (b) medium waves; (c) long waves.

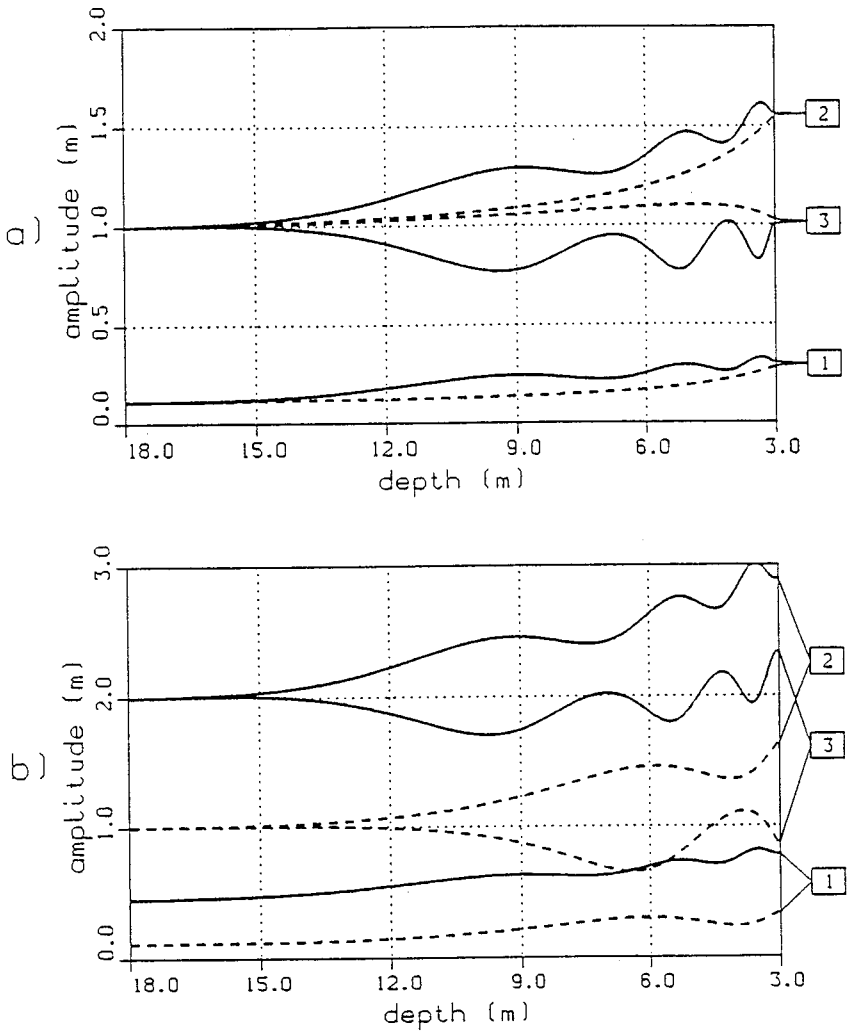

Fig. 4. Shoaling of a triad of waves (medium wavelength). (a) The influence of the slope. Full line: Slope 0.005, dashed line: Slope 0.05. (b) the influence of initial amplitudes (slope 0.01). Full line: Initial amplitudes 2 m. Dashed line: Initial amplitudes 1 m.

6. EXPERIMENTAL VERIFICATION

6.1. Laboratory experiments

The laboratory data used to test the present model consisted of measurements from the calibration tests for the Herzlia Marina model, conducted by Agnon and Keren (1990). The physical model replicates the bathymetry at the site, without the marina's structures. Simulations of shoaling of a modified JONSWAP spectrum (similar to the well known JONSWAP spectrum

but adjusted to regional conditions) were performed for various directions of propagation covering a wide range of characteristic spectral parameters (significant wave height, peak frequency). The wavemaker is a hydraulically controlled swaying vertical plate, programmable to a desired spectrum. Guiding walls were placed along wave characteristics on both sides in order to eliminate wall effects. Reflection from the beach was negligible.

The laboratory simulations were not designed specifically for the testing of the present model. For comparison purposes, we tried to choose the set of data which could be considered closest to the assumptions used in our derivation. The set chosen was that of waves approaching from the WNW direction (see Fig. 5), with significant wave height of 2 m and peak period of 14 s. It was closest to the direction of perpendicular incidence (about 5° off), and

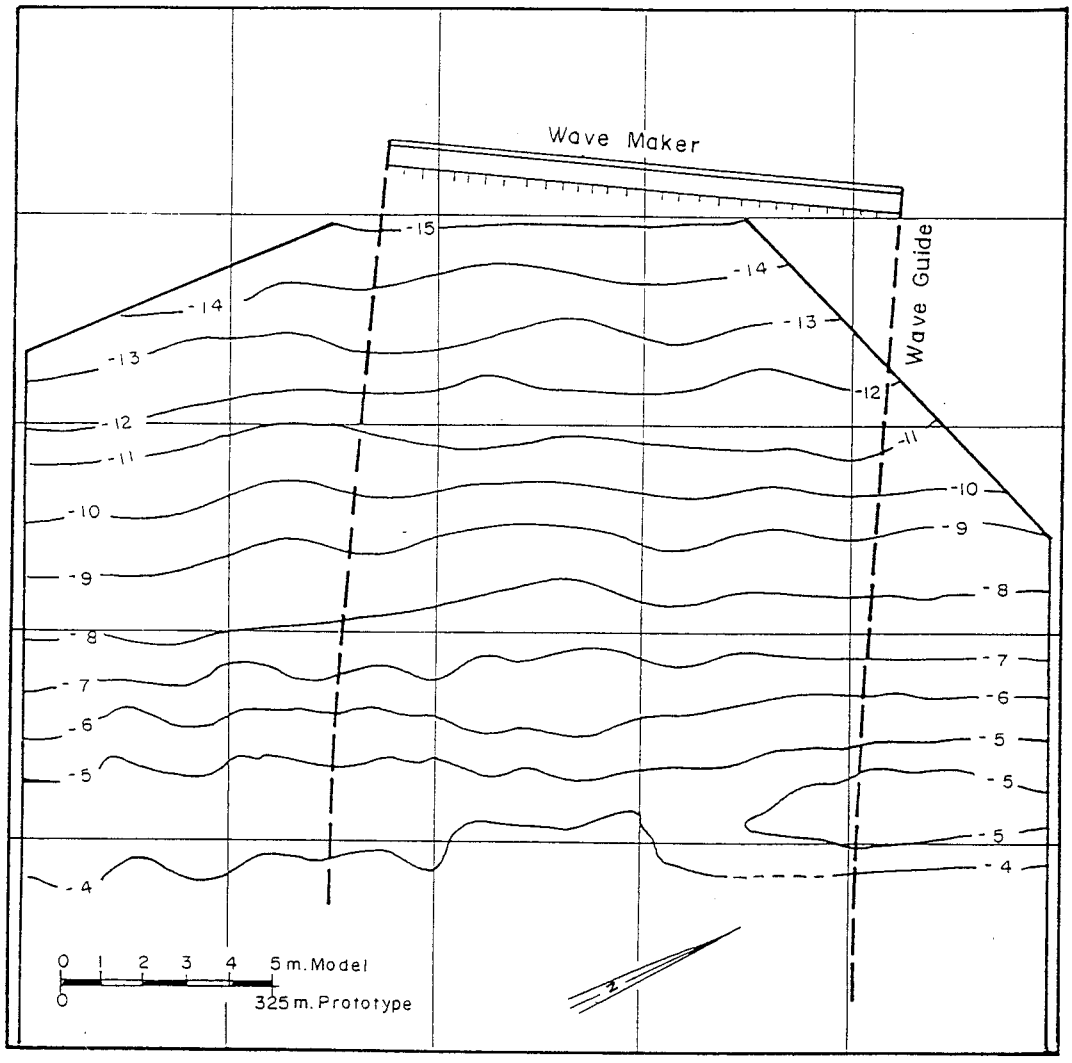

Fig. 5. Layout and bathymetry of laboratory simulations (Agnon and Keren, 1990). Depth contours in meters.

seemed to exhibit less wave breaking. Still some incompatibilities remain, which together with the inherent drawbacks of the present model, may account for some of the disagreement between the measured data and our numerical solution.

Among the important reasons for the discrepancies is the fact that the energy flux decreases in the experimental data (loss of energy through breaking), whereas the present model keeps the energy flux constant to 0.03 relative error. Also, the model does not account for possible excitation of the natural modes of oscillations of the basin, that should affect the domain of frequencies smaller than 0.03 Hz. Finally, and most important, no information on the modal initial phases was available, since it was suppressed in the spectral analysis process, in which a stochastic approach was employed.

The present model is a deterministic one, and the initial modal phases are of crucial importance for its description of the evolution of the shoaling spectrum. This crucial indeterminacy was tackled here by taking an ensemble of such initial random phases sets, with amplitudes that correspond to the measured spectrum, and averaging over the ensemble of results.

In the integrations, the slope of the bottom was taken 0.0118 which gives a total length of the shoaling domain of 845 m, for a difference of depth from 14 m to 4 m. In order to avoid the distortions introduced by the wavemaker, the model was initialized at 12 m depth. Discretization of the spectrum was made by defining (see Eq. 4.1):

$$\omega_n = n \cdot \Delta\omega \qquad n \text{ integer}, \ 1 \leqslant n \leqslant 60$$

$$\Delta\omega = \frac{1}{200}\text{Hz} \tag{6.1}$$

This set of frequencies was chosen in order to cover the frequency domain of the measured spectrum, and gives a reasonable balance of numerical effort and accuracy of description. The results presented in the figures are averages of over 50 sets of random initial phases. This number was also fixed by reasons of numerical effort.

In Fig. 6a, the measured spectrum at 12 m and 4 m depth is presented, together with the computed spectrum at 4 m. depth. The vertical span of the shaded area around the computed spectrum equals the modal standard deviation. Figure 6b shows, at the same depths as before the leading order energy flux spectra. As the linear theory keeps the modal energy flux exactly constant, the modifications of this spectrum are due only to nonlinear interactions. The area under the heavy and dashed curves is roughly the same. The effect of energy transfer to lower and higher frequencies is evident.

In order to obtain a global description of the accuracy of the numerical solutions, the frequency domain was divided into three regions approximately describing long, medium and short waves; significant wave heights

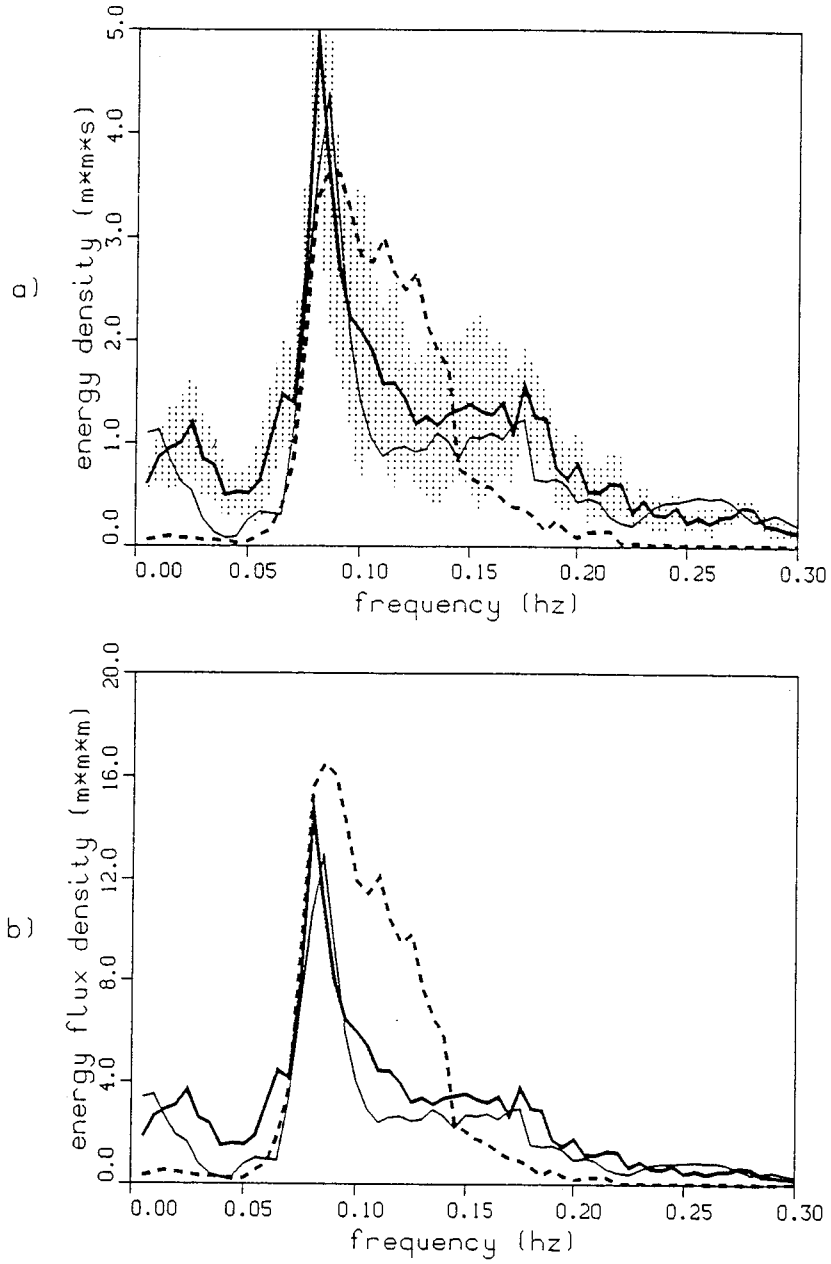

Fig. 6. Comparison of averaged numerical results (heavy line: results at 4 m depth) with laboratory measurements (dashed line: the initial spectrum at 12 m depth, thin line: the measured spectrum at 45 m depth). Vertical span of shaded area equals the modal standard deviation. (a) Energy spectrum; (b) leading order energy flux spectrum.

were calculated for each region, for the measured and computed shoaling spectra. Figure 7 shows the evolution of the computed spectrum in terms of these significant wave heights together with the ratios of the measured to computed heights. The main disagreements are for the total energy in the spectra at 6 and 4 m depth. Breaking of waves must have occurred there.

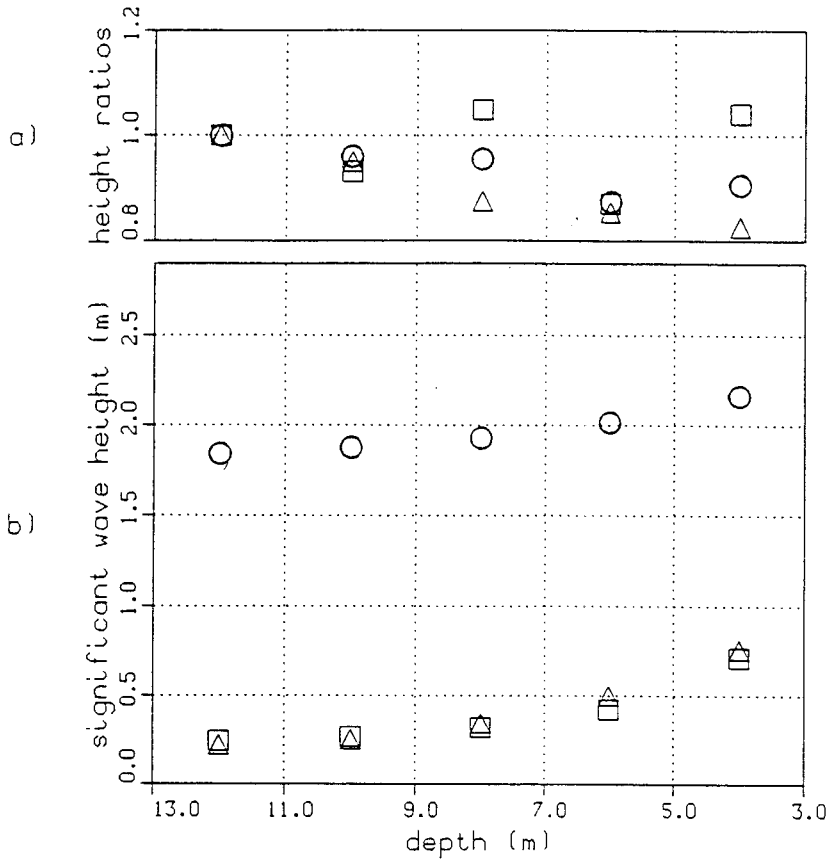

Fig. 7. The evolution of measured and computed significant wave heights for the comparison with laboratory measurements. (a) Ratios of measured to computed significant heights; (b) evolution of computed significant heights. (□) Long waves ($T > 20$ s); (△) short waves ($T < 5$ s); (○) total.

Although the model does not give an adequate description, in detail, of the processes in the very long wave domain, globally, in terms of significant wave heights, its prediction is rather close to the measurements, the error is less than 5% for depths greater than 6 m.

6.2. Field measurements

The present model was tested against field data provided by measurements conducted by CSIR (Division of Earth, Marine and Atmospheric Science and Technology) at Walker Bay, South Africa in February 1990. Again, the basic input to the numerical integrations were the spectral shapes, available at the depths of 19.3, 8.0, 6.3 m. The bottom slopes at the site are 0.019 and 0.011 for the first and second segments, respectively, corresponding to a total length of the considered shoaling domain of about 1000 meters. The bathymetry was closer to being two dimensional than the bathymetry in the laboratory exper-

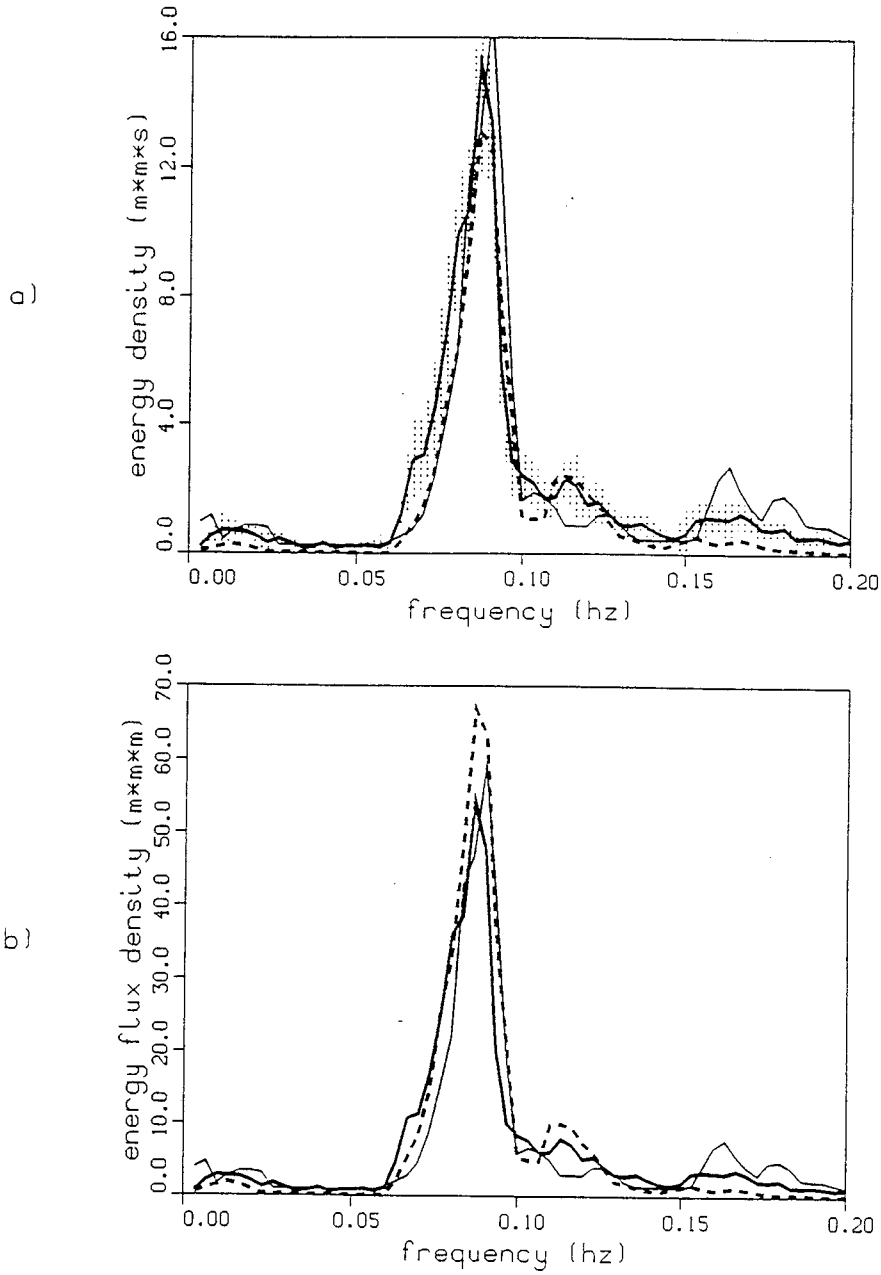

Fig. 8. Comparison of averaged numerical results (heavy line: results at 6.3 m depth) with field measurements (dashed line: the initial spectrum at 19.3 m depth, thin line: the measured spectrum at 6.3 m depth). Vertical span of shaded area equals the modal standard deviation. (a) Energy spectrum; (b) leading order energy flux spectrum.

iment above. The initial deviation from normal incidence was about 20° and decreased with the decreasing depth.

The initial spectrum (at 19.3 m depth) exhibits an energetic peak at a period of 10.8 s, and has a significant wave height of 2.14 m. Its evolution shows

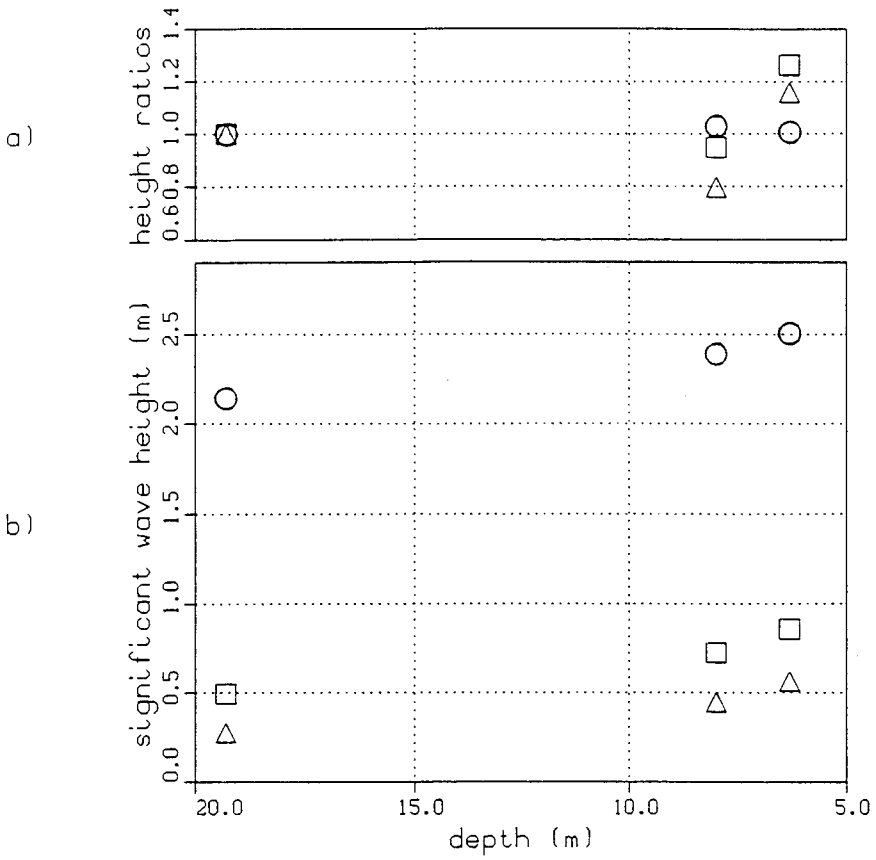

Fig. 9. The evolution of measured and computed significant wave heights for the comparison with field measurements. (a) Ratios of measured to computed significant heights; (b) evolution of computed significant heights. (□) Long waves ($T>20$ s); (△) short waves ($T<7$ s); (○) total.

the development of a secondary peak at the second harmonic of the peak frequency, and a weaker excitation of the long wave band. The first order energy flux, as calculated from the measurements, showed relative variations within the limit given by the errors of the numerical integrations (3%). This is in accordance also with the records of wave steepness, which indicate negligible wave breaking in the domain under consideration.

The numerical integrations were performed as for the case of laboratory measurements, but with a frequency resolution of $\Delta\omega = 1/300$ Hz (see Eq. 6.1), giving 60 modes for a high frequency cutoff at 0.2 Hz. Figs. 8 and 9 present the results averaged over 50 initial random phases sets.

The analysis in Figs. 8 and 9 follows that of Figs. 6 and 7, respectively. The spectrum measured at 19.3 m depth was used as input to the evolution equation of the present model and the results are compared with the measured spectrum at a depth of 6.3 m. The second harmonic at about 0.17 Hz is evident in the measurements more than in the computation. The diminishing of

the secondary peak at 0.11 Hz is also more pronounced in the measured data than in the model results.

As before, Fig. 8a presents the measured spectra at both ends of the shoaling domain, at 19.3 and 6.3 m depth, together with the computed spectrum at 6.3 m depth. Figure 8b presents at the same depths, the leading order energy flux spectra.

Figure 9 presents the evolution of the spectrum in terms of significant wave heights at the three locations. We see that the total significant wave height is within a 5% error bound.

6.3. Discussion

The performance of the model as compared with measurements is of great interest. For such a comparison, two sets of measured data were available to us — one coming from laboratory simulations, the other from field measurements, neither of them specifically designed for the testing of a deterministic unidirectional shoaling model. For the case of laboratory measurements, the bathymetry (Fig. 5) is nearly one dimensional, the waves do not propagate exactly normally to the shore, the data exhibit features that may be related to the excitation of the natural frequency of the basin, and the measured leading order energy flux shows a decrease of 20% at 4 m depth. Both sets of measurements provide input data for the model in the form of spectral shapes, with no information on the initial modal phases; information that is crucial for a deterministic model. This last difficulty was circumvented here by averaging over a large number of realizations (50 for each data set) performed with random initial phases. For a 60 modes spectrum, the total amount of C.P.U. time requested for the work on the IBM 3081D computer was about 12 hours. For each set of measurements, we calculated averages for separate sets of 15 runs each, in order to verify the consistency of the final results. Each such "partial" average yielded a fairly similar picture of the process (in terms of significant wave heights, the deviations with respect to the final "total" average over 50 integrations were not greater than 5%).

Bearing in mind the present simplifying assumptions which are not strictly valid for the data sets presented, the performance of the model is quite good. Further work should include comparison with data collected in unidirectional settings and mainly the extension of the model to more general situations, along the lines of the work of Suh et al. (1990) for Stokes waves.

ACKNOWLEDGEMENTS

This research was supported in part by CSIR Division of Earth, Marine and Atmospheric Science and Technology, Stellenbosch, South Africa, and by the fund for the promotion of research at the Technion and by Technion V.P.R.

fund — B. and N. Ginsburg Energy Research fund. We thank the reviewers for their comments. The manuscript was expertly typed by Ms. Ruth Adoni.

APPENDIX: SOLUTION OF THE LAPLACE EQUATION FOR THE VELOCITY POTENTIAL AND THE BOTTOM BOUNDARY CONDITION

Here we look for a solution of the system (3.8) in the form of an asymptotic expansion

$$F=F_1+i\epsilon F_2+O(\epsilon^2) \tag{A.1}$$

Substitution in Eq. (3.8) and separation of the powers of ϵ yields the following hierarchy:

$$(\epsilon^0)\quad \begin{cases} F_{1zz}-k^2F_1=0 & -h\le z\le 0 \\ F_{1z}-0 & z=-h \end{cases} \tag{A.2}$$

$$(\epsilon^1)\quad \begin{cases} F_{2zz}-k^2F_2=(kF_1)_{x_1}+kF_{1_{x_1}} & -h\le z\le \epsilon\eta \\ F_{2z}=kh_{x_1}F_1 & z=-h \end{cases} \tag{A.3}$$

The solution of Eq. (A.2) is simply:

$$F_1=f(x_1,\omega,t_1)\cosh k(z+h) \tag{A.4}$$

where f is an unknown function. Substitution of F_1 into Eq. (A.3) gives:

$$\begin{aligned} F_{2zz}-k^2F_2 &= 2kf_{x_1}\cosh k(z+h)+2k^2fh_{x_1}\sinh k(z+h) \\ &\quad +fk_{x_1}[2k(z+h)\sinh k(z+h)+\cosh k(z+h)] \qquad -h\le z\le\epsilon\eta \\ F_{2z} &= k_{x_1}f\cosh k(z+h) \qquad\qquad z=-h \end{aligned} \tag{A.5}$$

The solution of this system may be sought by means of variation of parameters. The following result is obtained:

$$\begin{aligned} F_2 &= [f_{x_1}(z+h)\sinh k(z+h)+fkh_{x_1}(z+h)\cosh k(z+h) \\ &\quad +\tfrac{1}{2}fk_{x_1}(z+h)^2\cosh k(z+h)] \end{aligned} \tag{A.6}$$

which may be rewritten as:

$$F_2=[f_{x_1}(z+h)\sinh k(z+h)+\tfrac{1}{2}fk(z+h)^2_{x_1}\cosh k(z+h)] \tag{A.7}$$

Defining the differential operator:

$$D(k,z)=i\left[(z+h)\sinh k(z+h)\frac{\partial}{\partial x_1}+\tfrac{1}{2}k(z+h)^2_{x_1}\cosh k(z+h)\right] \tag{A.8}$$

we may finally write the solution for F as:

$$F=f\cosh k(z+h)+\epsilon D(k,z)f \tag{A.9}$$

where f remains an unknown function:

$$f=f(x_1,\omega,t_1) \tag{A.10}$$

and may be written formally as:

$$f=\frac{1}{\cosh(kh)}\varphi(x_1,\omega,t_1) \tag{A.11}$$

This solution is used in Eqs. (3.9) and (3.10).

REFERENCES

Agnon, Y. and Keren, Y., 1990. Herzlia Marina Model Study, Calibration Tests. CAMERI — Coastal and Marine Engineering Research Institute, Technion City, Haifa, P.N. 245/90.

Armstrong, J.A., Bloemberg, N., Ducuing, J. and Pershan, P.S., 1962. Interaction between light waves in a nonlinear dielectric. Phys. Rev. B, 127: 1918–1939.

Bretherton, F.P., 1964. Resonant interactions between waves: The case of discreet oscillations. J. Fluid Mech., 20: 457–480.

Burlisch, R. and Stoer, J., 1966. Numerical treatment of ordinary differential equations by extrapolation methods. Num. Math. 8: 1–13.

Davey, A. and Stewartson, K., 1974. On three dimensional packets of surface waves. Proc. R. Soc. London A, 388: 101–110.

Djordjevic, V.D. and Redekopp, L.F., 1978. On the development of packets of surface gravity wave moving over an uneven bottom. J. Appl. Math. Phys. (ZAMP), 29: 950–962.

Freilich, M.H. and Guza, R.T., 1984. Nonlinear effects on shoaling surface gravity waves. Philos. Trans. R. Soc. London, A311: 1–41.

Grimshaw, R., 1970. The solitary wave in water of variable depth. J. Fluid Mech., 42: 639–656.

Laing, A.K., 1986. Nonlinear properties of random gravity waves in water of finite depth. J. Phys. Oceanogr., 16: 2013–2030.

Peregrine, D.H., 1967. Long waves on a beach. J. Fluid Mech., 27: 815–827.

Phillips, O.M., 1977. The Dynamics of the Upper Ocean. Cambridge University Press, Cambridge.

Stiassnie, M., 1983. Derivation of the nonlinear Schrödinger equation for shoaling wave-groups. J. Appl. Math. Phys. (ZAMP), 34: 534–544.

Suh, K.D., Dalrymple, R.A. and Kirby, J.T., 1990. An angular spectrum model for propagation of Stokes waves. J. Fluid Mech., 221: 205–232.

Whitham, G.B., 1974. Linear and Nonlinear Waves. Wiley-Interscience, New York.